Solar Energy 264 (2023) 112081

Contents lists available at ScienceDirect

Solar Energy

journal homepage: www.elsevier.com/locate/solener

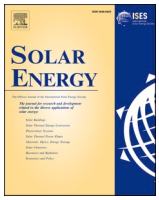

Core–shell structure selective emitter doped with rare earth elements for solar thermophotovoltaic system

Zongbin Hou [a], Hongyu Wang [a], Jiyu Wang [a], Yunpeng Liu [a,b], Xiaobin Tang [a,b,*], Kelum A.A. Gamage [c], Zhiheng Xu [a,b,*]

[a] Department of Nuclear Science and Technology, Nanjing University of Aeronautics and Astronautics, Nanjing 211106, China
[b] Key Laboratory of Nuclear Technology Application and Radiation Protection in Astronautics, Ministry of Industry and Information Technology, Nanjing 211106, China
[c] Centre for Educational Development and Innovation, James Watt School of Engineering, University of Glasgow, Glasgow G12 8QQ, UK

ARTICLE INFO

Keywords:
Solar thermophotovoltaic
Thermal emitter
Selective emission
InGaAs cell

ABSTRACT

Aiming at the low utilization of radiation photons in the solar thermophotovoltaic system, a rare earth core–shell (REC) structure selective thermal emitter is designed to achieve selective emission. The 3D symmetrical opal core–shell structure and rare earth elements play an important role in the selective emission characteristic of the REC emitter. The opal core–shell structure of the REC emitter is optimized by finite difference time domain simulation and numerical calculation, and the optimal size is determined. The REC emitter can adjust the characteristic peak of rare earth elements to produce a narrow–band radiation peak with an emissivity approaching 1 at a wavelength just before the cutoff wavelength, and maintain low emissivity in the long and short–wave bands. The conversion efficiency of the solar thermophotovoltaic system based on the REC emitter and InGaAs cell is 17.29 % at 1400 K, and the power density can reach 428.3 mW/cm^2. The mechanism of the selective emission characteristic of the REC emitter is revealed, and its emissivity is insensitive to polarization and incidence angle. The REC emitter further improves the selective emission characteristic and makes the radiation spectrum better match the thermophotovoltaic cell. The power density and conversion efficiency of the solar thermophotovoltaic system are increased by improving the utilization of the thermophotovoltaic cell to the radiation photon.

1. Introduction

With the increasing demand for energy, people are paying more attention to clean energy such as solar energy, which can be used in many ways. Solar thermophotovoltaic (STPV) technology converts the sunlight spectrum into near–infrared spectrum and generates electricity with infrared sensitive thermophotovoltaic (TPV) cells [1]. STPV has the unique advantages of high theoretical conversion efficiency, high power density, simple energy exchange structure, and high stability. STPV has very broad application and development prospects in the utilization of solar energy because the thermal emitter can reshape solar radiation spectrum and solve the problem of mismatch between the spectrum and the TPV cell [2–7].

The STPV system is mainly composed of absorber, thermal emitter, filter, and TPV cells, as shown in Fig. 1 (a). In operation, the absorber receives the sunlight, heats up, and transfers the heat to the thermal emitter. The high–temperature thermal emitter generates thermal radiation. The radiation photons hit TPV cells to generate electron hole pairs through the photovoltaic effect. When an external load is applied, electrons and holes migrate toward the two ends to generate current. However, not all photons can be absorbed and converted by TPV cells. Fig. 1 (b) shows only photons whose wavelength is shorter than the cutoff wavelength of TPV cells can be used and converted into electrical energy. Other photons cannot be converted but can heat TPV cells, causing adverse effects [8–10]. Moreover, because of the high thermal loss, the short–wave photon causes relatively low energy utilization efficiency [7,11–13]. Therefore, adjusting the radiation spectrum by optimizing the thermal emitter is the key to improve the performance of STPV system.

Early selective emitters were mainly material–based thermal emitters, which realized selective emission through the characteristics of the materials, such as yttrium oxide, erbium oxide, and other rare earth oxides or ceramics doped with metal ions [14–17]. Selective emitters using these materials can produce narrow–band emission peaks

* Corresponding authors at: Department of Nuclear Science and Technology, Nanjing University of Aeronautics and Astronautics, Nanjing 211106, China.
E-mail addresses: tangxiaobin@nuaa.edu.cn (X. Tang), xuzhiheng@nuaa.edu.cn (Z. Xu).

https://doi.org/10.1016/j.solener.2023.112081
Received 27 April 2023; Received in revised form 29 July 2023; Accepted 30 September 2023

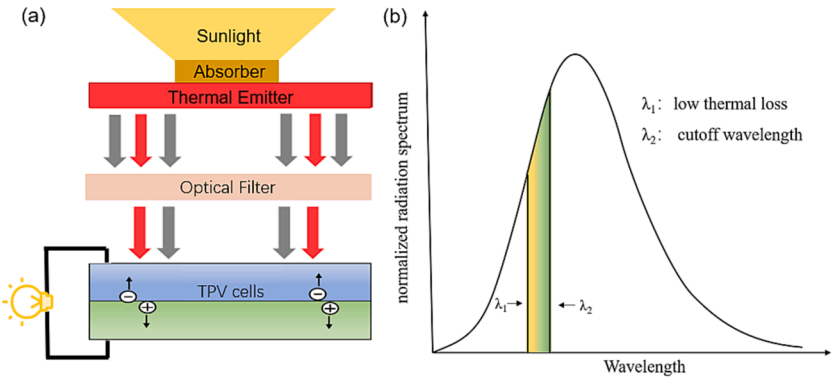

Fig. 1. (a) Structure and workflow of a STPV system. (b) Radiation spectrum of a blackbody emitter (solid black line) and an ideal thermal emitter (colored region).

determined by the characteristics of the materials themselves, but these characteristic peaks are often not within the optimal response range of TPV cells, and the problem of small view factor due to the distance between the emitter and TPV cells cannot be solved [18].

With the development of nanophotonic and micro–nano processing technology, the research on structure–based selective thermal emitter has gradually emerged, such as photonic crystals (PhC) and metamaterial (MTM) [11]. These selective emitters usually consist of materials with different refractive indices arranged periodically, ranging from 1D periodic structure to 3D symmetric structure [9,19–26]. The opal structure designed and applied in this paper is a representative 3D PhC structure. The symmetry in three directions makes the selective emitter exhibit emissivity insensitivity to polarization and incident angle. The core–shell structure, as a typical MTM, can use fully the different materials with large refractive index difference to regulate the radiation spectrum, which can be perfectly applied in the opal structure. Previous works designed a selective emitter with core–shell nanosphere structure using tungsten and SiO_2, and achieved relatively excellent selective emission characteristic [27]. However, the emitter still has high emissivity at short wavelength, which does not solve the problem of high thermal loss. Therefore, rare earth elements were introduced into the thermal emitter in this paper to solve the problem of efficiency reduction caused by the thermal loss of short–wave photons [16,28].

Based on the existing research of core–shell thermal emitter, rare earth elements were applied to play the characteristic peaks, and the 3D selective structure was used to adjust the characteristic peaks to the optimal response range of TPV cells, thus forming the selective emission characteristic of the thermal emitter. The rare earth core–shell (REC) emitter was simulated by using the finite difference time domain method. Through the design and optimization of its structure, the optimal performance was obtained, and the influence law of the REC emitter on the electrical performance of the STPV system was explored. The emissivity insensitivity to polarization and incident angle of the REC emitter was investigated, and the selective emission characteristic of the REC emitter was analyzed. Moreover, the REC emitter samples were prepared by using the wet chemical method. The aim of this study is to propose an emitter design with excellent selective emission characteristic and beneficial to improving the performance of STPV system.

2. Materials and methods

2.1. Structure design of REC emitter structure

Based on the 3D structure of opal, nanospheres were replaced with core–shell nanosphere structure, and rare earth elements were used in it to build the core–shell nanosphere of rare earth oxides (Y_2O_3 mainly used in this simulation) and SiO_2. The core–shell nanospheres were stacked to form a 3D opal structure, and a certain thickness of tungsten was used as the base plate at the bottom. The structural design of the REC emitter is shown in Fig. 2. The REC emitter combines the selective 3D structure with rare earth elements to produce a very narrow radiation peak in front of the InGaAs cutoff wavelength 1.72 μm, which is expected from the spectrum of the REC emitter. At the same time, the symmetrical 3D structure of the REC emitter makes it have emissivity insensitivity to polarization and incident angle. Aiming at the design of the REC emitter, the model is built in FDTD, the variation law of the thermal radiation performance with the Y_2O_3 radius R, SiO_2 thickness H and stacking layers N were explored, and the optimal structural size was determined by effective spectral efficiency as the evaluation basis.

2.2. Effective radiation spectrum calculation

The photon transmissivity $T(\lambda)$ is zero because the thickness at the bottom of the emitter is in the order of microns. According to Kirchhoff's law, when an object is in thermal equilibrium, its emissivity $\varepsilon(\lambda)$ at each wavelength is equal to the absorptivity $\alpha(\lambda)$, which can be calculated from the reflectance $R(\lambda)$:

$$\varepsilon(\lambda) = \alpha(\lambda) = 1 - R(\lambda) \tag{1}$$

The thermal radiation power at temperature T can be derived according to the blackbody radiation and the emissivity of the emitter $E_e(\lambda, T)$:

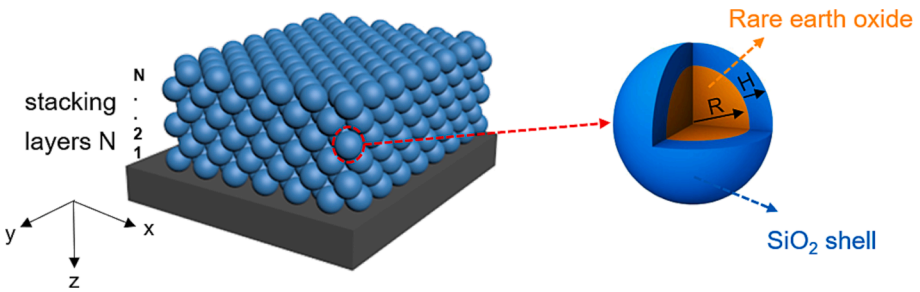

Fig. 2. Geometric structure design of the REC emitter.

$$E_e(\lambda,T) = E_b(\lambda,T)\varepsilon(\lambda) \tag{2}$$

$$E_b(\lambda,T) = \frac{2hc^2}{\lambda^5}\frac{1}{e^{\frac{hc}{\lambda kT}}-1} \tag{3}$$

where $E_b(\lambda,T)$ is the thermal radiation power of the blackbody at temperature T, which can be obtained by Planck's blackbody radiation law (Equation (3)), h is Planck's constant, c is the speed of light in vacuum, and k is Boltzmann's constant.

In order to evaluate the selective emission characteristic of the REC emitter, it is necessary to focus on whether the radiated photons can be used by the TPV cell as much as possible. The proportion η_t of photons whose wavelength is shorter than the cutoff wavelength in the radiation spectrum of the REC emitter can be derived from the emissivity $\varepsilon(\lambda)$ [29]:

$$\eta_t = \frac{\int_0^{\lambda_{TPV}} E_e(\lambda,T)d\lambda}{\int_0^{\infty} E_e(\lambda,T)d\lambda} \tag{4}$$

where λ_{TPV} is the cutoff wavelength of the TPV cell.

In addition to selective emission, the thermal radiation power of the emitter is also an important evaluation index. The proportion η_c of available radiation photons emitted by REC emitter to the available radiation photons emitted by blackbody can be calculated:

$$\eta_c = \frac{\int_0^{\lambda_{TPV}} E_e(\lambda,T)d\lambda}{\int_0^{\lambda_{TPV}} E_b(\lambda,T)d\lambda} \tag{5}$$

To evaluate the spectral modulation ability of the REC emitter, the effective spectral efficiency η_{sp} is used as the evaluation index. It can not only ensure the energy conversion efficiency of the TPV system, but also enable the system to have high power density. The calculation formula is as follow:

$$\eta_{sp} = \eta_t\eta_c \tag{6}$$

2.3. Performance of STPV system

InGaAs cell was used for electrical output in the STPV system. To calculate the electrical output of the InGaAs cell, the photon number density $n(\lambda,T)$ radiated by the REC emitter is obtained, which can be derived according to emissivity $\varepsilon(\lambda)$:

$$n(\lambda,T) = \frac{2\pi c}{\lambda^4}\frac{\varepsilon(\lambda)}{e^{\frac{hc}{\lambda kT}}-1} \tag{7}$$

When the radiation photons hit TPV cells, the resulting short–circuit current J_{sc} and reverse saturation current J_0 can be calculated from the quantum efficiency η_{EQE} of TPV cells:

$$J_{SC} = q\int_0^{\lambda_{TPV}} n(\lambda,T)\eta_{EQE}(\lambda)d\lambda \tag{8}$$

$$J_0 = q\int_0^{\lambda_{TPV}} \frac{2\pi c}{\lambda\left[exp\left(\frac{hc}{\lambda kT}\right)-1\right]}d\lambda \tag{9}$$

According to Shockley formula, the output current density $J(V)$ generated by the photovoltaic effect in TPV cells can be calculated. The calculation formula is as follow:

$$J(V) = J_{SC} - J_0\left[exp\left(\frac{qV}{kT_\alpha}\right)-1\right] \tag{10}$$

where q is the unit charge, V is the output voltage, and T_α is the TPV cell temperature, which is set as 300 K.

At this time, the maximum output power of the STPV system P_{max} is determined by the maximum product of the output current density and the output voltage:

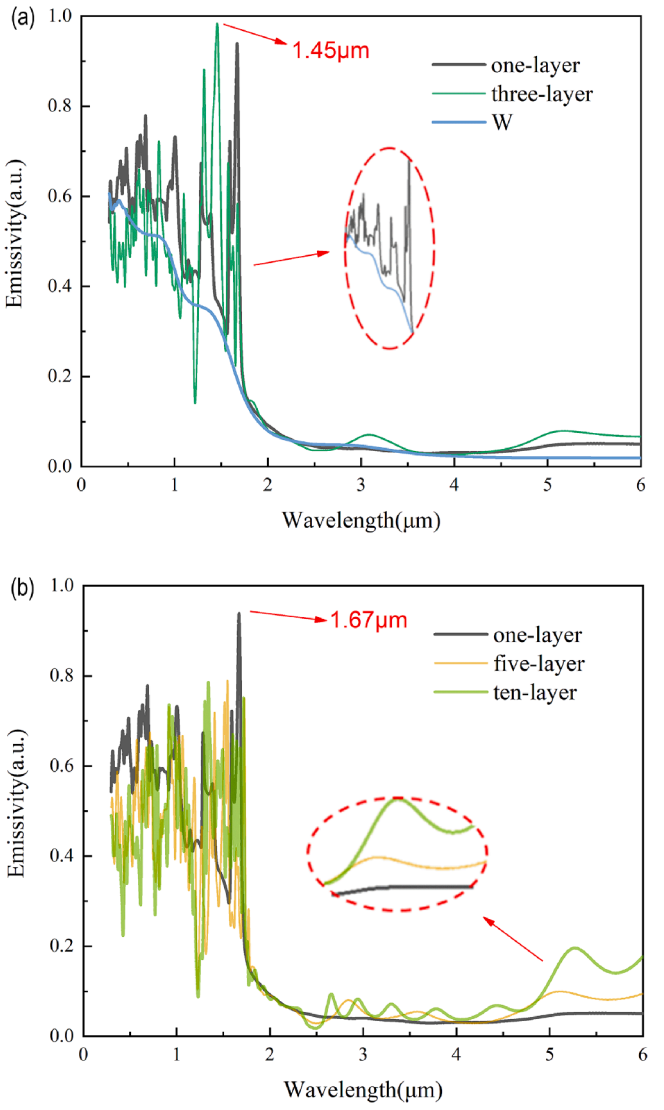

Fig. 3. (a) Emissivity of the REC emitter with 1 or 3 layers and the flat tungsten emitter. (b) Emissivity of the REC emitter with 1, 5, or 10 layers.

$$P_{max} = Max(V \times J) \tag{11}$$

Therefore, the system efficiency of the STPV system η_{sys} can be calculated by the following formula:

$$\eta_{sys} = \frac{P_{max}}{\int_0^{\infty} E_e(\lambda,T)d\lambda} \tag{12}$$

2.4. Fabrications of REC emitter

REC emitter samples were prepared by solution method. 150 mL ethanol solution (99.7 %, AR) was added with 1 g Er_2O_3 or Y_2O_3 and ultrasonic dispersed for 1 min, followed by 7 g polyvinylpyrolidone (PVP) and ultrasonic dispersed again for 1 min. The mixed solution of the two was magnetically stirred for 24 h, in which PVP was used as a dispersant to stabilize the rare earth oxide nanoparticles and prevent their aggregation. The solution was then centrifuged and washed several times. The washed rare earth oxides and 6 mL 3–aminopropyl trethoxysilane (APS) were added to 150 mL ethanol solution, respectively, and ultrasonic dispersion was carried out twice for 1 min before and after. After 24 h of magnetic stirring, the solution was centrifuged several times. APS was used as a surface modifier to change the nanoparticles so that the outer layer can be coated with SiO_2 shell. Then, rare earth

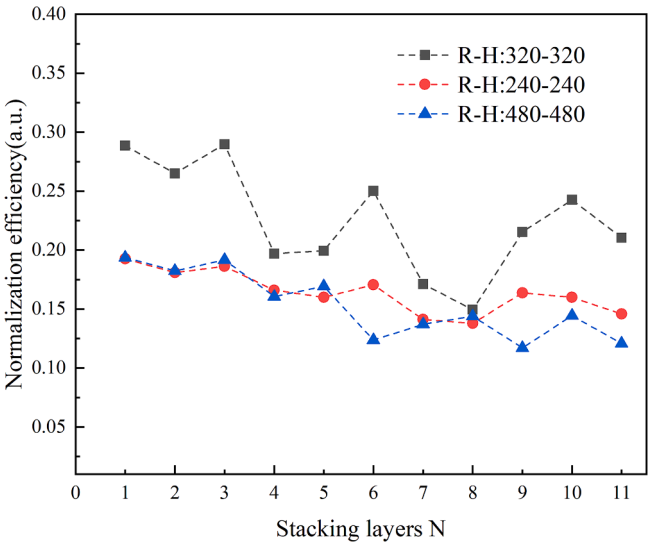

Fig. 4. Effective spectral efficiency of the REC emitter with the number of layers.

oxides were added to 150 mL ethanol solution, and 1 mL ammonia water was added to make the solution alkaline. The mixed solution was magnetically stirred for 12 h, and 0.5 mL tetraethyl orthosilicate (TEOS, 99 %, GC) was dripped four times (once every 3 h) to provide SiO_2 for the system through the hydrolysis polycondensation reaction. The final solution was centrifuged, washed, and dried into sample powder, and then the REC emitter sheet was cold pressed by a tablet press under 8 MPa pressure.

3. Results and discussions

3.1. Emissivity of REC emitter

The emissivity of the REC emitter obtained through simulation with FDTD is shown in Fig. 3 (a, b). When the wavelength is lower than the cutoff wavelength, the emissivity of the REC emitter oscillates in the range of 0.4–0.8, whereas the emissivity drops rapidly to zero after the cutoff wavelength. Its emissivity is substantially better than that of flat tungsten emitter. The REC emitters with one–layer and three–layer structures generate a narrow–band emission peak with an emissivity close to 1 near the cutoff wavelength, whereas other layers, such as 5 and 10 layers, do not have this emission peak. The emission peaks at 1.45 and 1.67 μm are within the optimal response range of the InGaAs cell, which is the most important selective emission characteristic, and the energy conversion efficiency is the highest at this time. Moreover, the thermal emitter with high stacking layers has weaker inhibition on long–wave band emissivity.

Fig. 4 shows the effective spectral efficiency gradually decreases with the increase of accumulation layer number *N* overall, and an oscillation is observed during the decline. Owing to its emissivity peak before cutoff wavelength, the effective spectral efficiency of the REC emitter has a peak value at one and three–layer structures with all size combinations. When the two conditions are compared, the one–layer REC emitter has a better emissivity suppression effect at the long wavelength. Photons with wavelengths longer than the cutoff wavelength only heat TPV cells adversely, so the one–layer REC emitter is more effective at weakening the energy loss caused by low–energy photons.

The influences of the core radius *R* and the core–shell thickness *H* were further explored based on the one–layer REC emitter. First, the parameters of 100, 160, 240, 320, 480, and 640 nm were combined as *R* and *H* pairs to form 36 kinds of nanosphere structures for simulation. The size was selected corresponding to the optimal value from the

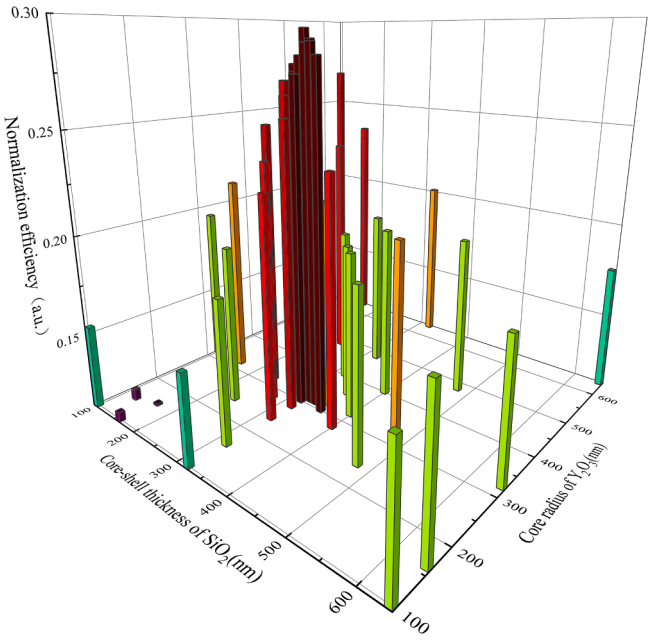

Fig. 5. Effective spectral efficiency of the one–layer REC emitter with the core radius *R* and the core–shell thickness *H*.

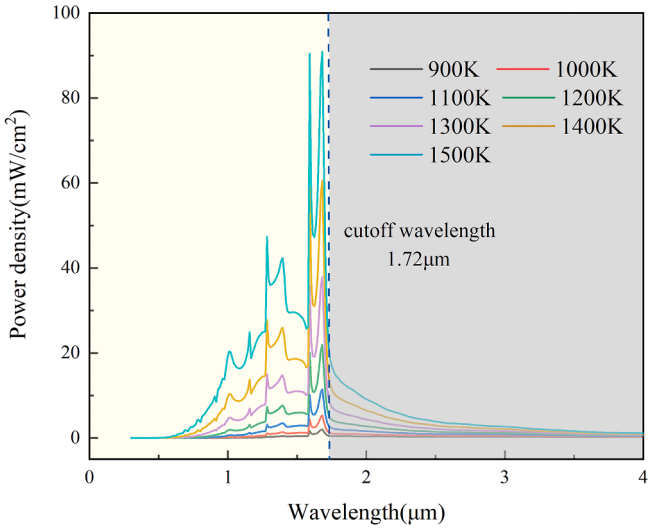

Fig. 6. Thermal radiation power density spectrum of optimal size REC emitter.

simulation results, eight samples were used by dichotomy between the optimal value and the suboptimal value for simulation, and the above steps were repeated. After four dichotomies, a simulated sample whose size gradually approached the optimal value can be obtained in Fig. 5. The effective spectral efficiency obtained from the whole simulation sample at the temperature of 1300 K gradually increased from around to the middle, and the best effective spectral efficiency can reach 29.48 % (The flat tungsten emitter of the same thickness was 15.12 %), which was obtained when $R = 330$ nm and $H = 310$ nm. This is the optimal REC emitter size matching InGaAs cutoff wavelength of 1.72 μm.

3.2. Analysis of electrical output

Fig. 6 shows the power density spectrum of the optimized Y_2O_3@SiO_2 REC emitter at different temperatures. The thermal radiation power density of the REC emitter at different temperatures presents the same change trend. The REC emitter can maintain low thermal

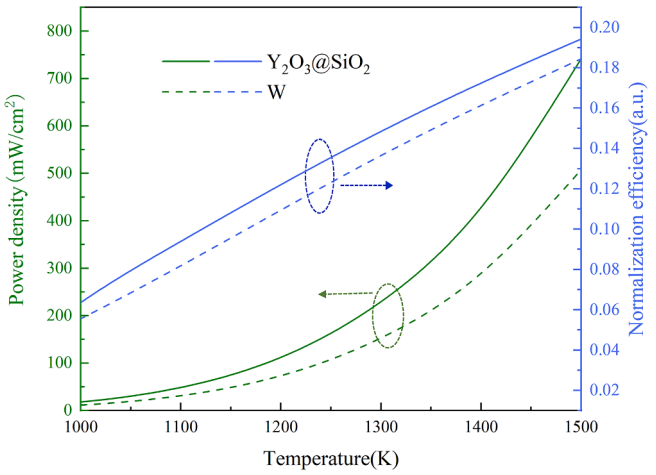

Fig. 7. Power density and conversion efficiency of the two thermal emitters with temperature.

Table 1
Power density of REC emitters Y_2O_3@SiO_2 and Er_2O_3@SiO_2 (mW/cm^2).

REC emitter	Emitter temperature		
	900 K	1100 K	1300 K
Y_2O_3@SiO_2	0.5026 ± 0.004	12.44 ± 0.24	55.734 ± 4.29
Er_2O_3@SiO_2	1.3504 ± 0.047	28.986 ± 1.21	69.202 ± 2.55

radiation in short wavelengths. Although these photons can be used by the TPV cell, their utilization efficiency is very low. Because a rather large proportion of photon energy is wasted in the form of heat. The low radiation in short wavelengths can further improve the conversion efficiency of the STPV system. In addition, when the wavelength exceeds 1.72 μm, the radiation power density decreases rapidly and becomes zero. If these photons are absorbed by the TPV cell, they will not be converted into electric energy, and they will heat up the TPV cell, which will have adverse effects. Therefore, keeping the radiation low in the long wavelength range can well eliminate the energy loss generated by the photons outside the band gap. Finally, a high narrow peak can be clearly seen at 1.59–1.70 μm. The radiation peak is within the optimal response range of InGaAs cell, and the conversion efficiency of TPV cells is highest in this wavelength band. This narrow–band radiation peak is the advantage of rare earth elements used in REC emitter, which can maximize the energy conversion efficiency of radiated photons. These results indicate the core–shell structure changes the wavelength of radiated photons through the refractive index difference, and the rare earth elements show their narrow–band radiation characteristics well. Further doping with rare earth elements on the basis of core–shell selective emitter can substantially improve selective emission characteristic.

By using the thermal radiation power density spectrum of the REC emitter combined with the quantum efficiency of InGaAs cell, the *I–V* and *P–V* curves of the STPV system can be calculated, and the power density and conversion efficiency are shown in Fig. 7. The performance of plate tungsten emitter is simulated under the same conditions. With the increase of temperature, the power density and conversion efficiency of the two thermal emitters increase gradually, which is consistent with the simulation results. The conversion efficiency of the REC emitter is slightly higher than that of the flat tungsten thermal emitter, which are 17.29 % and 16.17 %, respectively at 1400 K. The power density of the system can reach 428.3 mW/cm^2 when the REC emitter is used, which is 1.48 times that of flat tungsten.

The prepared REC emitter is combined with InGaAs cell to build STPV system for testing. The power density of the system at 900 K, 1100 K, and 1300 K is shown in Table 1. The output of the sample prepared with Er_2O_3 is slightly higher than that of Y_2O_3, and the power density of the STPV system is 55.73 ± 2.15 mW/cm^2 and 69.20 ± 1.27 mW/cm^2 at 1300 K.

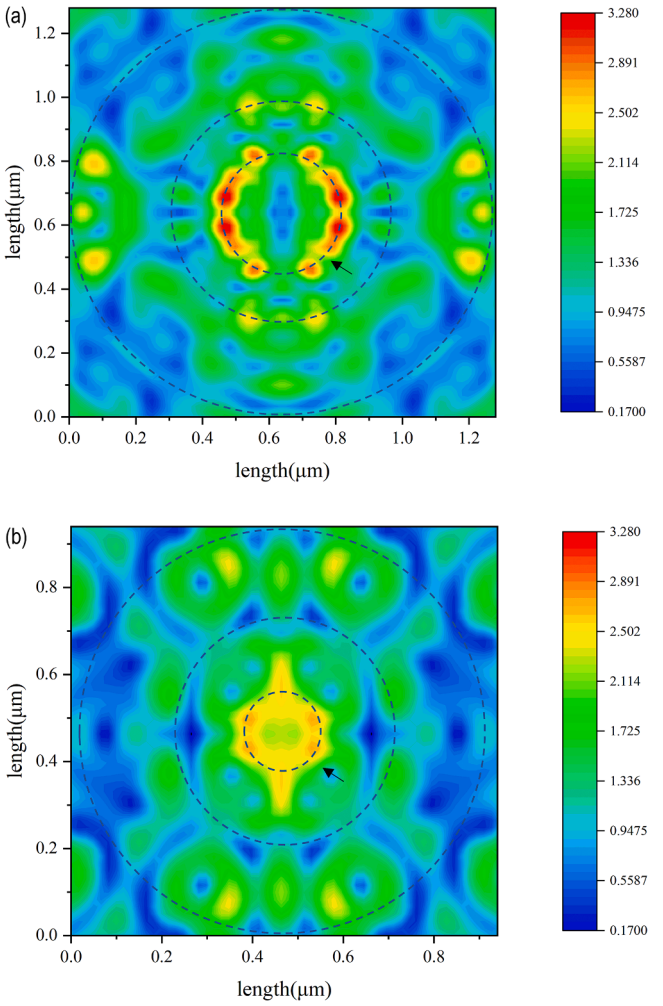

Fig. 8. Electric field distribution of REC emitters with size (a) R = 330 nm, H = 310 nm (b) R = 240 nm, H = 240 nm.

3.3. Radiation characteristics and mechanism of REC emitter

To analyze the selective emission mechanism of the REC emitter further, the electric field distribution of the REC emitter with the optimal structure size (R–H = 330 nm–310 nm) and the contrast structure size (R–H = 240 nm–240 nm) in FDTD are drawn in Fig. 8. The two larger dotted lines are the boundaries of Y_2O_3 and SiO_2. The strongest electric fields are mostly located on the dotted line of the arrow, inside the rare earth oxide. This factor is the most important one affecting the ultra–high narrow–band radiation peak of the REC emitter before the cutoff wavelength. The core–shell structure adjusts the characteristic peak of rare earth elements to the optimal response range of the InGaAs cell, so that rare earth elements can make a great contribution to the narrow–band radiation peak of the REC emitter. Second, the sub–strong electric field is distributed on the SiO_2 surface, and the distribution of the electric field restricted in the dielectric layer is a typical characteristic of magnetic polariton resonance. Magnetic polariton resonance also determines the selective emission characteristic of the REC emitter, which is the advantage of using core–shell structure in REC emitters. Finally, the distribution of the electric field is symmetric, which macroscopically makes the REC emitter insensitive to

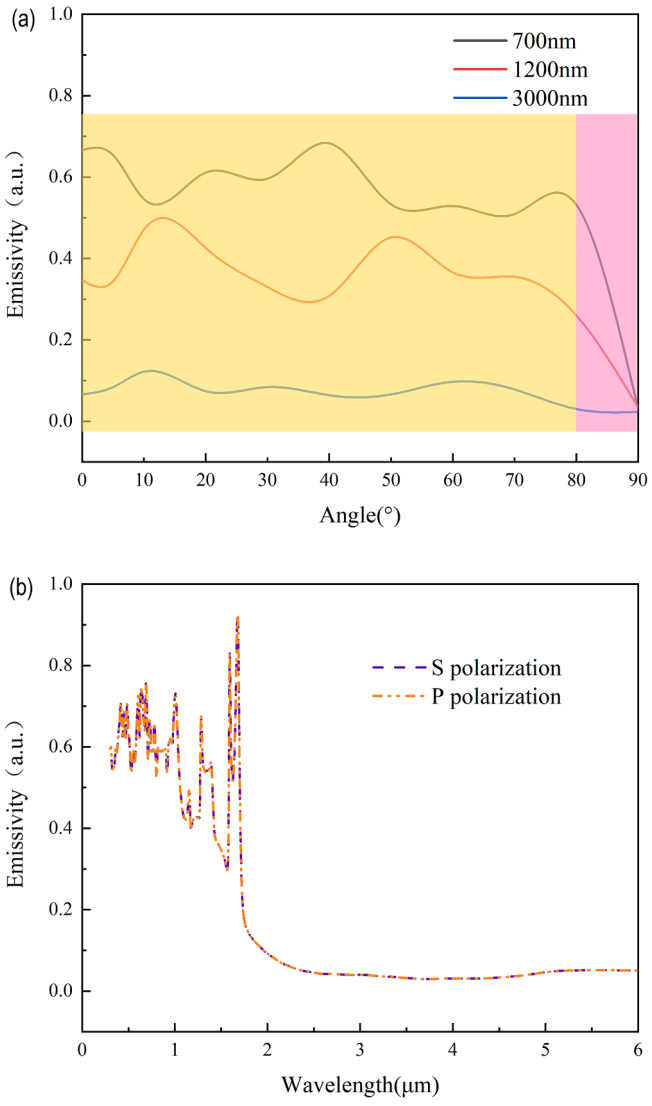

Fig. 9. Emissivity of the REC emitter (a) with the angle of incidence and (b) at different polarizations.

polarization and incident angles.

Fig. 9 (a) shows the emissivity curves of heat–radiated light of different wavelengths at dissimilar incidence angles. When the incidence angle is between 0° and 80°, the emissivity stays within a certain range, and decreases rapidly to zero after 80°. The structural design has emissivity insensitivity to incident angle and can maintain the selective emission characteristic up to 80° of incident angle. Fig. 9 (b) shows the emissivity spectra of the REC emitter under different polarized light. For S polarization and P polarization, the emissivity of the REC emitter is same, and it has polarization insensitivity. In the actual work of the thermal emitter, the thermal radiation light in different incidence angles must meet the selective emission characteristic needed. The designed 3D symmetrical structure can make the REC emitter have emissivity insensitivity to polarization and incident angle until 80°. The REC emitter can maintain excellent selective emission characteristic under most system structural designs and small view factor.

4. Conclusion

In this paper, a core–shell selective emitter doped with Y_2O_3 was designed, and its structure was optimized. The optimization results show rare earth elements can exert the typical peak characteristics in the REC emitter well, so that the emissivity is concentrated in front of the TPV cell cutoff wavelength. Moreover, the application of core–shell structure can further adjust the characteristic peaks of rare earth elements, so that the emission peaks are concentrated in the optimal response band of InGaAs cells, while maintaining a very low emissivity in the long and short–wave bands. Therefore, the REC emitter has good selective emission characteristic, and the STPV system combined with InGaAs cells has high conversion efficiency. The effective spectral efficiency is up to 29.48 %, and the system conversion efficiency is 17.29 % at 1400 K. In addition, the emissivity of the REC emitter has emissivity insensitivity to polarization and incident angle until 80°, which can solve the problem of small view factor due to spacing in practical applications. These results demonstrate the designed REC emitter can further improve the performance of STPV system, and introduce some experience and technology for the development of subsequent high–efficiency STPV system.

Declaration of Competing Interest

The authors declare that they have no known competing financial interests or personal relationships that could have appeared to influence the work reported in this paper.

Acknowledgments

This work is supported by the National Natural Science Foundation of China (Grant Nos. 12075119 and 12275132), the Natural Science Foundation of Jiangsu Province (Grant No. BK20201288), the China Postdoctoral Science Foundation (Grant No. 2022M711613), the Excellent Postdoctoral Program of Jiangsu Province (Grant No. 2022ZB235), and the Postgraduate Research & Practice Innovation Program of NUAA (Grant No. xcxjh20220622).

References

[1] R. Bhatt, I. Kravchenko, M. Gupta, High–efficiency solar thermophotovoltaic system using a nanostructure–based selective emitter, Sol. Energy 197 (2020) 538–545, https://doi.org/10.1016/j.solener.2020.01.029.
[2] A. Datas, A. Martí, Thermophotovoltaic energy in space applications: review and future potential, Sol. Energy Mater. Sol. Cells 161 (2017) 285–296, https://doi.org/10.1016/j.solmat.2016.12.007.
[3] Wang, Y., Liu, H., Zhu, J., 2019. Solar thermophotovoltaics: progress, challenges, and opportunities. Appl. Mater. 7, 080906. https://doi.org/10.1063/1.5114829.
[4] C.M.I. Hussain, A. Duffy, B. Norton, Thermophotovoltaic systems for achieving high–solar–fraction hybrid solar–biomass power generation, Appl. Energy 259 (2020), 114181, https://doi.org/10.1016/j.apenergy.2019.114181.
[5] S. Shan, Q. Zhang, B. Chen, G. He, S. Jia, Z. Zhou, Effect evaluation of micro/nano structured materials on the performance of solar thermophotovoltaic system: An analysis based on measurement data, Sol. Energy 231 (2022) 1037–1047, https://doi.org/10.1016/j.apenergy.2019.114181.
[6] J. Tian, S. Shan, B. Chen, Z. Zhou, Y. Zhang, Parametrical analysis of a novel solar cascade photovoltaic system via full–spectrum splitting and residual–spectrum reshaping, Sol. Energy 243 (2022) 120–133, https://doi.org/10.1016/j.solener.2022.07.046.
[7] S. Wen, A. Bhaskar, Improving the performance of solar thermophotovoltaic (STPV) cells with spectral selected absorbers and small apertured radiation shields, Int. J. Heat Mass Transf. 184 (2022), 122266, https://doi.org/10.1016/j.ijheatmasstransfer.2021.122266.
[8] C. Ogbonnaya, A. Turan, C. Abeykoon, Numerical integration of solar, electrical and thermal exergies of photovoltaic module: A novel thermophotovoltaic model, Sol. Energy 185 (2019) 298–306, https://doi.org/10.1016/j.solener.2019.04.058.
[9] C. Jiang, H. Huang, Z. Zhou, Enhancement in the multi–junction thermophotovoltaic system based on near–field heat transfer and hyperbolic metamaterial, Sol. Energy 217 (2021) 390–398, https://doi.org/10.1016/j.solener.2021.01.074.
[10] B. Roy-Layinde, T. Burger, D. Fan, B. Lee, S. McSherry, S.R. Forrest, A. Lenert, Sustaining efficiency at elevated power densities in InGaAs airbridge thermophotovoltaic cells, Sol. Energy Mater. Sol. Cells 236 (2021), 111523, https://doi.org/10.1016/j.solmat.2021.111523.
[11] Z. Wang, D. Kortge, Z. He, J. Song, J. Zhu, C. Lee, H. Wang, P. Bermel, Selective emitter materials and designs for high–temperature thermophotovoltaic applications, Sol. Energy Mater. Sol. Cells 238 (2021), 111554, https://doi.org/10.1016/j.solmat.2021.111554.

[12] Z. Zhou, Q. Chen, P. Bermel, Prospects for high–performance thermophotovoltaic conversion efficiencies exceeding the Shockley-Queisser limit, Energ. Conver. Manage. 97 (2015) 63–69, https://doi.org/10.1016/j.enconman.2015.03.035.
[13] Q. Wang, Z. Huang, J. Li, G.Y. Huang, D. Wang, H. Zhang, J. Guo, M. Ding, J. Chen, Z. Zhang, Z. Rui, W. Shang, J.Y. Xu, J. Zhang, J. Shiomi, T. Fu, T. Deng, S. G. Johnson, H. Xu, K. Cui, Module–level polaritonic thermophotovoltaic emitters via hierarchical sequential learning, Nano Lett. 23 (2023) 1144–1151, https://doi.org/10.1021/acs.nanolett.2c03476.
[14] N. Nakagawa, H. Ohtsubo, Y. Waku, H. Yugami, Thermal emission properties of $Al_2O_3/Er_3Al_5O_{12}$ eutectic ceramics, J. Eur. Ceram. Soc. 25 (2005) 1285–1291, https://doi.org/10.1016/j.jeurceramsoc.2005.01.031.
[15] M.C. Mesa, P.B. Oliete, R.I. Merino, V.M. Orera, Selective thermo–emission in directionally solidified Al_2O_3–$Er_3Al_5O_{12}$ and Al_2O_3–$Er_3Al_5O_{12}$–ZrO_2 eutectics, J. Eur. Ceram. Soc. 33 (2012) 2587–2596, https://doi.org/10.1016/j.jeurceramsoc.2013.05.001.
[16] H. Lian, Z. Hou, M. Shang, D. Geng, Y. Zhang, J. Lin, Rare earth ions doped phosphors for improving efficiencies of solar cells, Energy 57 (2013) 270–283, https://doi.org/10.1016/j.energy.2013.05.019.
[17] R. Sakakibara, V. Stelmakh, W.R. Chan, M. Ghebrebrhan, J.D. Joannopoulos, M. Soljačić, I. Čelanović, Practical emitters for thermophotovoltaics: a review, J. Photon. Energy 9 (2019), 032713, https://doi.org/10.1117/1.JPE.9.032713.
[18] E. López, I. Artacho, A. Datas, Thermophotovoltaic conversion efficiency measurement at high view factors, Sol. Energy Mater. Sol. Cells 250 (2023), 112069, https://doi.org/10.1016/j.solmat.2022.112069.
[19] B. Zhao, L. Wang, Y. Shuai, Z.M. Zhang, Thermophotovoltaic emitters based on a two–dimensional grating/thin–film nanostructure, Int. J. Heat Mass Transf. 67 (2013) 637–645, https://doi.org/10.1016/j.ijheatmasstransfer.2013.08.047.
[20] J. Song, H. Wu, Q. Cheng, J. Zhao, 1D trilayer films grating with $W/SiO_2/W$ structure as a wavelength–selective emitter for thermophotovoltaic applications, J. Quant. Spectrosc. Radiat. Transf. 158 (2015) 136–144, https://doi.org/10.1016/j.jqsrt.2015.02.002.
[21] D.N. Woolf, E.A. Kadlec, D. Bethke, A.D. Grine, J.J. Nogan, J.G. Cederberg, D. B. Burckel, T.S. Luk, E.A. Shaner, J.M. Hensley, High–efficiency thermophotovoltaic energy conversion enabled by a metamaterial selective emitter, Optica 5 (2018) 213, https://doi.org/10.1364/OPTICA.5.000213.
[22] Z. Yang, S. Ishii, A.T. Doan, S.L. Shinde, T.D. Dao, Y. Lo, K. Chen, T. Nagao, Narrow–band thermal emitter with titanium nitride thin film demonstrating high temperature stability, Adv. Opt. Mater. 8 (2020) 1900982, https://doi.org/10.1002/adom.201900982.
[23] Z. Zhou, C. Jiang, H. Huang, L. Liang, G. Zhu, Three–junction tandem photovoltaic cell for a wide temperature range based on a multilayer circular truncated cone metamaterial emitter, Energy 210 (2020), 118503, https://doi.org/10.1016/j.energy.2020.118503.
[24] C. Dong, Y. Zheng, K.S. Shen, H.C. Liu, S.Q. Xia, J. Zhang, H. Lu, X.Z. Zhang, Y. F. Liu, Polarization–independent wide–angle flexible multiband thermal emitters enabled by layered quasi–periodic photonic crystal, Opt. Laser Technol. 156 (2022), 108474, https://doi.org/10.1016/j.optlastec.2022.108474.
[25] B. Chen, S. Shan, J. Liu, Z. Zhou, An effective design of thermophotovoltaic metamaterial emitter for medium–temperature solar energy storage utilization, Sol. Energy 231 (2022) 194–202, https://doi.org/10.1016/j.solener.2021.11.067.
[26] B. Chen, S. Shan, J. Liu, A novel molten salt energy storage–solar thermophotovoltaic integrated system with mid–temperature metamaterial spectrum reshaping, Sol. Energy Mater. Sol. Cells 243 (2022), 111799, https://doi.org/10.1016/j.solmat.2022.111799.
[27] C. Meng, Y. Liu, Z. Xu, H. Wang, X. Tang, Selective emitter with core–shell nanosphere structure for thermophotovoltaic systems, Energy 239 (2022), 121884, https://doi.org/10.1016/j.energy.2021.121884.
[28] N.A. Pfiester, T.E. Vandervelde, Selective emitters for thermophotovoltaic applications, Phys. Status Solidi A 214 (2017) 1600410, https://doi.org/10.1002/pssa.201600410.
[29] L. Mo, L. Yang, E.H. Lee, S. He, High–efficiency plasmonic metamaterial selective emitter based on an optimized spherical core–shell nanostructure for planar solar thermophotovoltaics, Plasmonics 10 (2015) 529–538, https://doi.org/10.1007/s11468-014-9837-6.